Journal of Power Sources 267 (2014) 515–520

Contents lists available at ScienceDirect

Journal of Power Sources

journal homepage: www.elsevier.com/locate/jpowsour

Investigations on degradation of the long-term proton exchange membrane water electrolysis stack

Shucheng Sun [a, b], Zhigang Shao [a, *], Hongmei Yu [a], Guangfu Li [a], Baolian Yi [a]

[a] Fuel Cell System and Engineering Laboratory, Dalian Institute of Chemical Physics, Chinese Academy of Sciences, 457 Zhongshan Road, Dalian, Liaoning 116023, PR China
[b] University of the Chinese Academy of Sciences, Beijing 100039, China

HIGHLIGHTS

- Degradation of electrolysis stack after running 7800 h is investigated.
- Cations occupied ion exchange sites of membrane and the catalyst layers.
- Cations impurities cause the increase in ohmic resistance and charge transfer resistance.
- The hydrogen crossover rate of the MEA slightly increased after 7800 h operation.
- Cell performance is almost completely recovered after dilute sulfur acid treatment.

ARTICLE INFO

Article history:
Received 26 March 2014
Received in revised form
21 May 2014
Accepted 22 May 2014
Available online 2 June 2014

Keywords:
Proton exchange membrane
Water electrolysis stack
Degradation
Cation contamination

ABSTRACT

A 9-cell proton exchange membrane (PEM) water electrolysis stack is developed and tested for 7800 h. The average degradation rate of 35.5 μV h^{-1} per cell is measured. The 4th MEA of the stack is offline investigated and characterized. The electrochemical impedance spectroscopy (EIS) shows that the charge transfer resistance and ionic resistance of the cell both increase. The linear sweep scan (LSV) shows the hydrogen crossover rate of the membrane has slight increase. The electron probe X-ray microanalyze (EPMA) illustrates further that Ca, Cu and Fe elements distribute in the membrane and catalyst layers of the catalyst-coated membranes (CCMs). The cations occupy the ion exchange sites of the Nafion polymer electrolyte in the catalyst layers and membrane, which results in the increase in the anode and the cathode overpotentials. The metallic impurities originate mainly from the feed water and the components of the electrolysis unit. Fortunately, the degradation was reversible and can be almost recovered to the initial performance by using 0.5 M H_2SO_4. This indicates the performance degradation of the stack running 7800 h is mainly caused by a recoverable contamination.

1. Introduction

The extensive consumption of fossil fuels over the last century and the associated perspectives of short-term supply shortages are calling for new, clean and cheap technologies. Hydrogen may play an important role as an energy carrier of the future [1]. Proton exchange membrane (PEM) water electrolysis is potentially interesting for the decentralized production of hydrogen from renewable energy sources [2,3], which offers a convenient and efficient way to produce hydrogen.

Compared to the conventional alkaline process, PEM water electrolysis offers a number of advantages for the production of electrolytic grade hydrogen, such as higher efficiency and reliability, higher gas purity (above 99.99%), and the possibility of producing compressed gases (up to 150 bar and more) for direct pressurized storage without any external mechanical compression [4,5].

Most research papers published in the open literatures on the subject focused on corrosion-resistive current collector [6–8], novel anode or cathode catalysts [9–13]. Although the long-term stability studies for the water electrolysis stack are of crucial importance from the view point of the industrial application, few publications are available concerning the degradation of PEM electrolysis stack [14,15].

* Corresponding author. Tel.: +86 411 84379153; fax: +86 411 84379185.
E-mail address: zhgshao@dicp.ac.cn (Z. Shao).

http://dx.doi.org/10.1016/j.jpowsour.2014.05.117
0378-7753/

Millet et al. [14] fabricated a GenHy1000 stack and measured its performances. Although the performances almost maintained stable during the first 800 h of operation, they observed performance degradation over longer periods of time. The contamination of metallic cations in the feed water and the degradation of the MEAs were the main causes of performance degradation. Selamet et al. [15] developed and optimized a 10-cell stack, the initial efficiency and performance of the stack was tested. But only a single cell was tested for 2000 h continuously and an degradation rate of 1.5 μV h^{-1} was measured. Wei G Q et al. [16] investigated the stability of a MEA with 4 cm^2 active area in a single electrolyzer for 208 h, they indicated the short period performance decline of the MEA was mainly caused by a recoverable contamination.

In this research, the water electrolysis stack was fabricated and the long-term durability was tested. The performance degradation was investigated after 7800 h operation and the contamination sources was also identified by using different characterizations methods. Recovery of the electrolysis performance was obtained by means of dilute sulfur acid treatment.

2. Experimental

2.1. Preparation of MEAs

Membrane electrode assemblies (MEAs) were prepared by using the catalyst-coated membrane (CCM) technique, as follows. Pt/C (40 wt%, Johnson matthey, HiSPECTM 4000) was used as hydrogen evolution reaction (HER) electrocatalyst for the cathode, and Iridium black (Johnson matthey, HiSPECTM 160000) was used as oxygen evolution reaction (OER) electrocatalyst for the anode. To prepare a catalyst layer, a homogeneous ink composed of electrocatalyst, a Nafion solution (5 wt%, E.I. DuPont de Nemours and Company) and isopropanol was sprayed directly onto the each side of a Nafion 115 membrane (DuPont, thickness: 127 μm, conductivity: 0.10 S cm^{-1} minimum). The electrocatalysts loading were 1.5 mg cm^{-2} Ir black and 0.4 mg cm^{-2} Pt, respectively. The Nafion loading in the catalyst layer was approximately 0.6 mg cm^{-2} for the hydrogen side and the oxygen side. To form a MEA for water electrolysis, the prepared CCM was hot-pressed with a carbon paper (Toray, TGP-H-060) together at 140 °C under a pressure of 1 MPa for 1.0 min. The effective area of the MEA was about 160 cm^2.

2.2. Water electrolysis stack

A 9-cells stack (hydrogen production capacity up to 0.3 Nm^3 H_2 h^{-1}) with 160 cm^2 active area per cell was designed and constructed, which was series connected in a filter-press configuration and used to investigate the durability. In the stack, porous titanium disks (Porosity: 40%, provided by Xi'an Baode Powder Metallurgy Co., Ltd.,China) electroplated Pt (Suzhou Borui Industrial Material Science & Technology Co., Ltd., China) were used as the anodic current collector, a carbon paper (Toray, TGP-H-060) was used as the cathode current collector and 40 mesh titanium grids electroplated Pt (Suzhou Borui Industrial Material Science & Technology Co., Ltd., China) were used as the spacers. Silicon rubber gaskets (thickness: 0.6 mm) were used as the cell sealants. Both the endplates and the bipolar plates were made of titanium alloy (TC4, thickness: 20 mm, Baoti Group Co., Ltd., China) and titanium foils (TA2, thickness: 0.2 mm, Baoti Group Co., Ltd., China), respectively.

2.3. Evaluation of water electrolysis stack

A self-made test station was employed to implement the long-term test of the water electrolysis stack, as given in Fig. 1. During the operation of water electrolysis, deionized water (Milli-Q, 18.2 MΩ cm resistivity) was pumped into the anode side of the stack from the bottom of water tank and flowed back to the top of water tank. The tank was also used as the separator of water and oxygen. The total water flow was 1.8 L min^{-1} and the average flow rate was 200 ml min^{-1} per cell. The DC power source (KIKUSUI PAT60-133T) provided an voltage on the electrolysis stack. Both H_2 and O_2 produced were evacuated. The water electro-dragged was separated in the cathode separator and reflowed to the bottom of the anode seperator. A desalinization cartridge was used before the water was fed to the electrolysis stack. The feed water was heated

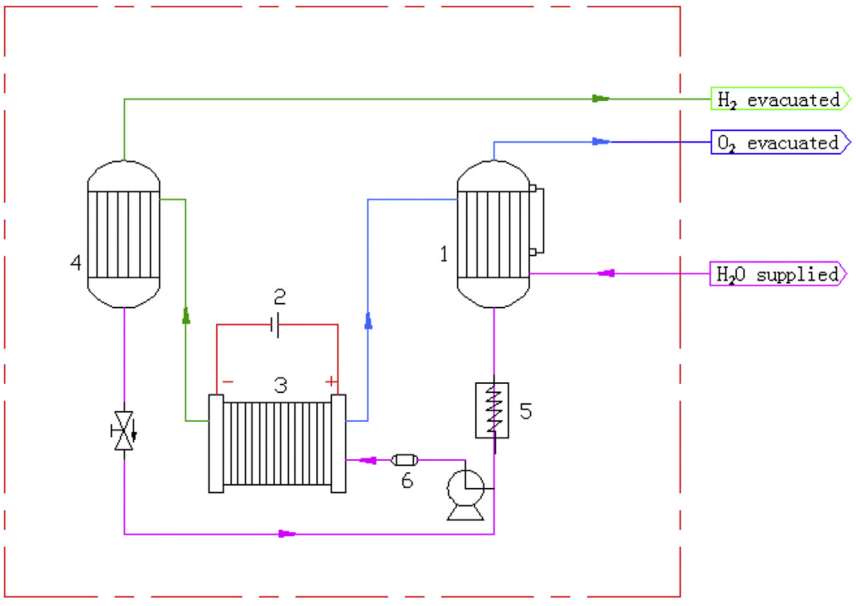

Fig. 1. Schematic sketch of test station for water electrolysis. 1. water tank; 2. DC power source; 3. electrolysis stack; 4. cathode separator; 5. heat exchanger; 6. desalinization cartridge.

by the heat exchanger and the stack temperature was kept at 60 °C. The stack was operated galvanostatically at 0.5 A cm^{-2} and atmospheric pressure. In order to ensure continuous operation, water was supplemented from the deioned water (Milli-Q) reservior. The voltage and current were measured and recorded automatically by means of a data acquisition card (PCI-1711L, Advantech, Taiwai) and computer.

2.4. Samples preparation

In the next characterization, the 4th MEA of the 7800 h's stack was investigated. The samples were cut from the 4th MEA, which were named as MEA-7800 and MEA-7800 Renewed before and after recovered treatment, respectively, and the fresh MEA was named as MEA-0. The effective area of the MEAs were all 4 cm^2. During the recovered process, the MEA was immersed into 0.5 M sulfuric acid solution for 2 h, then the H_2SO_4 solution was poured out and the remaining MEA was washed off (6–8 times) using deioned water (Milli-Q), then immersed into deioned water for 2 h again.

2.5. Electrochemical characterization

2.5.1. Cyclic voltammogram (CV) and linear scan voltammogram (LSV) measurements

CV and LSV diagnostic tests were used to measure the electrochemical area (ECA) of the anode electrode and H_2 gas crossover rate by a PARSTAT 2273 instrument, respectively. The anode was fed in with the humidified H_2 worked as the counter and reference electrode, and the cathode fed in with ultrapure N_2 worked as the working electrode. CV measurements was performed at a rate of 50 mV s^{-1} in the voltage region of 0–1.2 V, and LSV measurements was performed at a rate of 4 mV s^{-1} in the voltage region of 0–0.6 V. The CV and LSV were measured at room temperature. The effective area of the MEAs was 4 cm^2.

2.5.2. I–V measurement

Prior to *I–V* measurements, the cells were operated at 0.5 A cm^{-2} for 30 min, which were tested at 60 °C and atmosphere pressure, and water was fed in 50 ml min^{-1} to the anode of the cells. The effective area of the MEAs was 4 cm^2. The *I–V* curves of the cells were galvanostatically measured using a DC supply, the data was measured and recorded automatically.

2.5.3. Electrochemical impedance spectroscopy (EIS) measurement

Prior to EIS measurements, the cells were operated at 0.5 A cm^{-2} and 60 °C for 30 min. EIS of the water electrolyzers were conducted at 1.55 V using a Solartron (1287A + 1260) in a range of frequency (0.1 Hz–10 kHz), and a 5 mA amplitude of current perturbation was employed.

2.5.4. Electrode potential measurement

The anode and cathode electrode potentials were measured against a saturation mercury electrode (SCE, 0.242 V vs. SHE). As it was mentioned in Ref. [17], this could be done by extending the piece of Nafion membrane contained in the MEA, and making the piece immerse in the 0.5 M H_2SO_4 solution. Using this method, the ionic contact was assured through forming a bridge between the MEA and H_2SO_4 solution. The anode and cathode electrode potentials could be automatically measured and recorded by means of computer and PCL-1711 card of Advantech company. One of the leads was connected to the electrolyzer anode or cathode and the second was connected to the SCE. The electrode potentials were measured against SCE and finally calibrated against SHE.

2.6. ICP and EPMA characterization

The distribution of cation impurities in the cross section of the MEAs was investigated by a Electron Probe X-ray Microanalyzer (EPMA-1600). The water of tank was analyzed by using inductance coupling plasma spectroscopy (ICP) at 0 h and 7800 h, respectively.

3. Results and discussion

3.1. Stability test

The experiments were performed to investigate the stability of a 9-cell PEM stack for 7800 h. The measured voltage of the stack varying with running time is shown in Fig. 2. According to Fig. 2, the voltage curve can be approximately divided into four regions. In first region of 0–4805 h, the voltage increases gradually from 14.16 V to maximum value 17.07 V, the fit curve illustrates the degradation rate is 0.589 mV h^{-1}. In second region of 4805–5094 h, the voltage nearly keeps stable. Whereas, in third region of 5094–6075 h, the voltage dramatically decreases from 17.05 V to 16.55 V in the rate of 0.512 mV h^{-1}, suggesting the enhanced cell performance. At last, the electrolysis voltage almost levels off (ca. 16.65 V). The average degradation rate of the individual cell voltage is around 35.5 μV h^{-1} during 7800 h life. In order to understand the observed degradation of stack performance, the 4th MEA was offline analyzed.

3.2. I–V curves analysis

As can be seen from Fig. 3, *I–V* curves of MEA-0, MEA -7800 and MEA -7800 Renewed were investigated. The performance of MEA -7800 is obviously worse than that of MEA-0 and MEA -7800 Renewed, the voltage increases from initial 1.61 V–1.897 V at 0.5 A cm^{-2} after 7800 h operation. After recovery treatment, MEA -7800 Renewed performs nearly as good as the fresh MEA in Fig. 3. The cell voltage recovers from 1.897 V to 1.624 V at 0.5 A cm^{-2}, which almost attains 99.1% initial performance. The result displays that the performance deterioration is reversible after 7800 h operation and can be recovered by dilute sulfuric acid.

3.3. Electrode potential analysis

To investigate the cause of performance degradation, the potential of the anode and cathode was measured, respectively. As

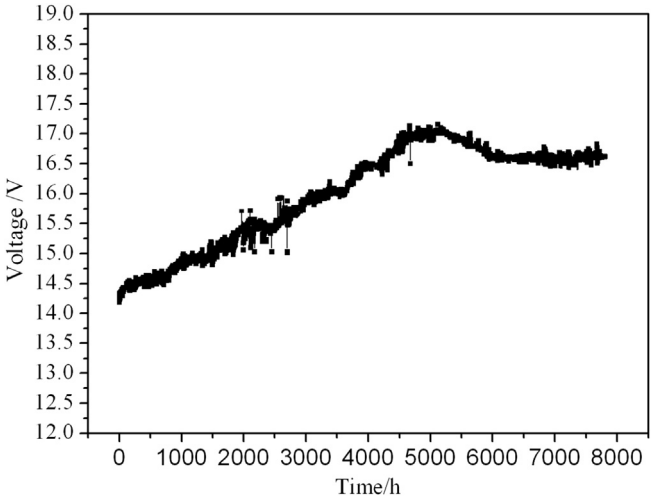

Fig. 2. Stack voltage varying with running time of water electrolysis during long-term operation.

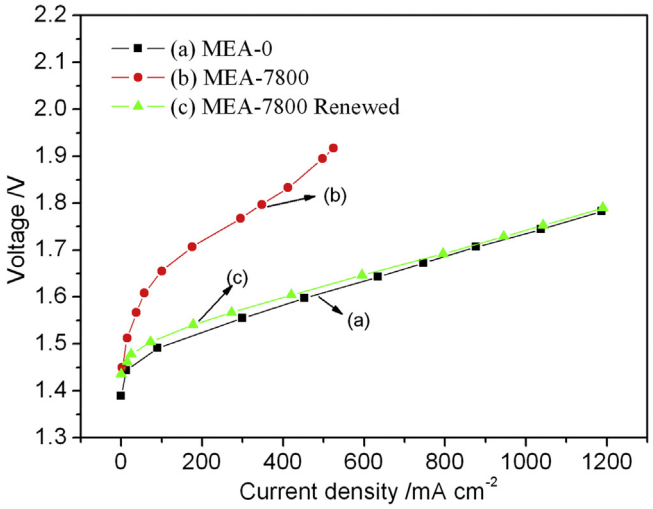

Fig. 3. Comparison of *I–V* curves for (a) MEA-0, (b) MEA-7800 and (c) MEA-7800 Renewed.

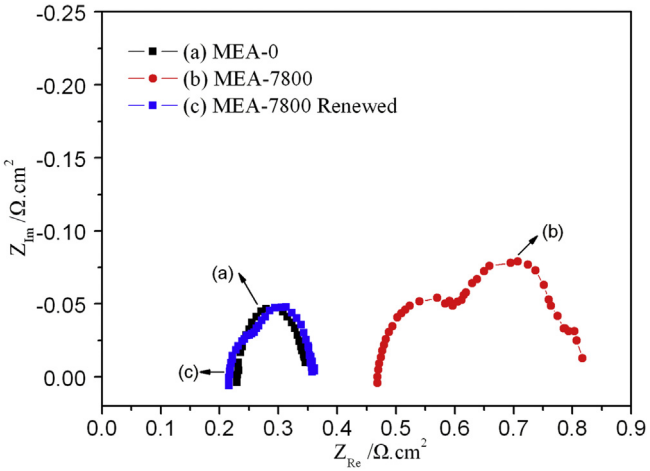

Fig. 5. EIS spectra of (a) MEA-0; (b) MEA-7800 and (c) MEA-7800 Renewed.

displayed in Fig. 4, the electrode potential of MEA-7800 is visibly worse than that of MEA-0 and MEA-7800 Renewed. The cathode potential of MEA-7800 decreased from −0.06 V to −0.2 V in the range of 0–530 mA cm^{-2}, and its anode potential increased from 1.44 V to 1.68 V in Fig. 4(b and e). However, the anode and cathode potentials of MEA-0 and MEA-7800 Renewed were almost uniform in the range of 0–1000 mA cm^{-2}, as shown in Fig. 4. The cell voltage is the potential difference between the anode and cathode potentials. Consequently, the dramatic variations of cell voltage in Fig. 2 is mainly attributed to the change of the anode and cathode overpotentials. But the cell performance can be almost completely recovered by the treatment using 0.5 M sulfuric acid solution. Accordingly, it can be deduced that the removable contaminants have influence on the anode and cathode reaction.

3.4. Electrochemical impedance spectrum (EIS) analysis

To get more insights into the performance degradation, the electrochemical impedance of the three electrolyzers was carried out at 1.55 V Fig. 5 shows Nyquist plots of the three electrolyzers. The high frequency intercepting with the real axis R_Ω of the cell

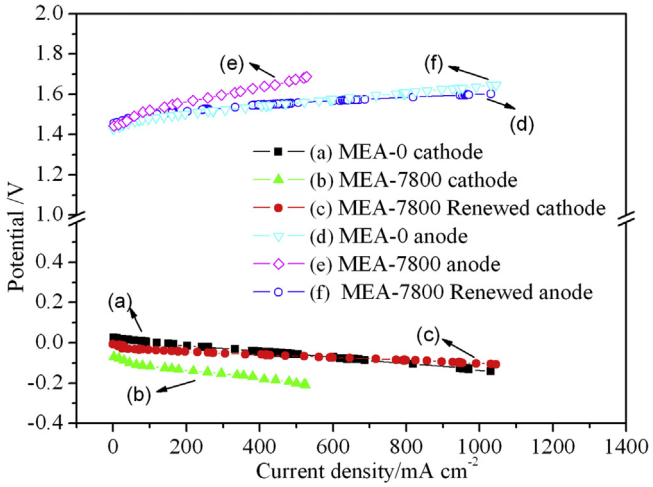

Fig. 4. The cathode and anode potential varying with current density from (a, d) MEA-0; (b, e) MEA-7800; (c, f) MEA-7800 Renewed.

using MEA-7800, which represents the total ohmic resistance after running 7800 h, is bigger than that of MEA-0 and MEA-7800 Renewed. Moreover, the arc diameter of the cell using MEA-7800 represents charge transfer resistance R_{ct} [18], which is also bigger than that of MEA-0 and MEA-7800 Renewed. The R_Ω and R_{ct} can be obtained through simulation with $R_\Omega(R_1Q_1)$ $(R_{ct}Q_{dl})$ equivalent circuit [19] and listed in Table 1. As shown in Table 1, both R_Ω and R_{ct} of MEA-7800 (Fig. 5(b)) obviously increase, therein R_{ct} is a distinct increase than R_Ω, which about triples that of MEA-0 (Fig. 5(a)). After recovery (Fig. 5(c)), R_Ω and R_{ct} are decreased and almost arrive at the initial value. Based on the agglomerate model, the microstructure of the porous catalyst layer can be depicted as catalyst particles covered with Nafion polymer electrolyte [20,21]. The catalyst and electrolyte provides catalytic sites and delivery channel of protons, respectively. According to our previous works [22], impurities will not only increase ohmic resistance but also hinder protons leave or transfer to the catalytic sites, which leads to the increase in charge transfer resistance R_{ct} and the decrease in exchange current density [23,24]. We can see from Table 1, the charge transfer resistance R_{ct} accounts for 34% in the total resistance for MEA-0, whereas it increases to 42.7% for MEA-7800. Thus it will lower the reaction rate and increase the overpotential at a given current density. After recovery (Fig. 5(c)), more protons are available in membrane and the three phase boundary of catalyst layers. That is the very reason for the recovered performance of MEA-7800 Renewed.

3.5. Cyclic voltammograms (CV) analysis

The performance of the anode catalyst was investigated using cyclic voltammograms (CV). We can see from Fig. 6, the CVs of MEA-7800 and MEA-7800 Renewed display the characteristic expansion in comparison with that of MEA-0. The increase in the total integral charge after 7800 h is ascribed to the gradual oxidation of Ir atoms available in the catalyst layer, which leads to hydration of the iridium oxide and increase of the number of active

Table 1
Impedance parameters obtained through fitting the experimental data to the $R_\Omega R_1Q_1(R_{ct}Q_{dl})$ circuit.

Sample	MEA − 0	MEA − 7800	MEA − 7800 Renewed
R_Ω (Ω cm^2)	0.23	0.47	0.22
R_{ct} (Ω cm^2)	0.12	0.35	0.14

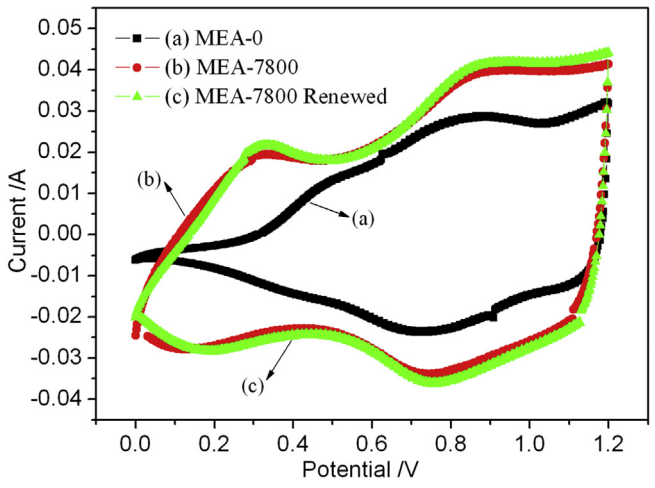

Fig. 6. Cyclic voltammograms of (a) MEA-0; (b) MEA-7800 and (c) MEA-7800 Renewed.

sites accessible for the electrochemical reaction [25]. The peaks are broad and not very well depicted, suggesting an existence of variety of active surface sites with different formal potentials, which is consistent with the amorphous state of the iridium oxide [25]. In addition, a pair of broad peaks for MEA-7800 sit at the potential range of around 0.6 V–1.0 V vs. SHE. Particularly, the anodic peak of MEA-7800 localizes 0.78 V–1.1 V vs. SHE, and the peak is approximately horizontal, which is attributed to the Ir(III)/Ir(I) and Ir(V)/Ir(VI) redox surface transition [26]. An increase of the peaks of Ir(III)/Ir(IV) and Ir(V)/Ir(VI) redox surface transition is observed after 7800 h, which may be attributed to an increase of the number of active surface sites. This also indicates that the contaminants do not cover with active surface sites in the anode catalyst layer and only occupy the ion exchange sites in the catalyst layers. Moreover, the evident Pt peaks are observed at the anode, which may be attributed to the trace amount of porous titanium disc electroplated Pt draining into anode catalyst during the long-term operation.

3.6. Hydrogen crossover rate

Fig. 7 shows the hydrogen crossover rate of the membrane before and after 7800 h operation. The hydrogen crossover rate can be determined using the plateau current density at voltage above 0.35 V, where the current density obtained is limited by the hydrogen transport rate through the membrane [27]. As shown in Fig. 7, the hydrogen crossover current density increases slightly from 1.28 mA cm^{-2} (Fig. 7(a)) to 1.56 mA cm^{-2} after 7800 h operation (Fig. 7(b)). Due to the pressure results in the membrane thin during the fabrication process, which would increase the hydrogen crossover rate of the membrane to a certain extent.

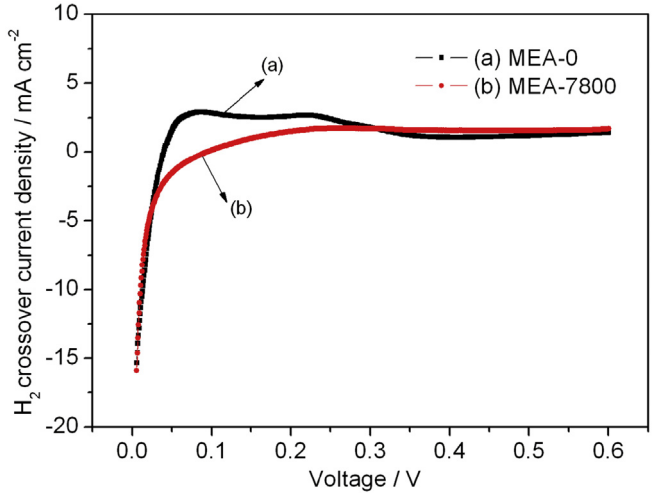

Fig. 7. H_2 crossover rate of the membrane of (a) MEA-0; (b) MEA-7800.

3.7. Electron probe microanalysis (EPMA)

Fig. 8 shows the EPMA (electron probe microanalysis) results at the cross-section of the CCMs (the catalyst-coated membrane) from MEA-0, MEA-7800 and MEA-7800 Renewed. The distributions of Ca, Cu and Fe were analyzed. Compare to Fig. 8(a) and (c), the elements content in the membrane and anode catalyst layer shows higher relative intensity in Fig. 8(b), whereas it increases slightly in the cathode catalyst layer. This can be attributed to the low content of Nafion polymer electrolyte in the cathode catalyst layers and higher affinity of cations than protons for the sulfonic acid group sites [28–30], which also proves that metallic cations migrates from the anode to the cathode [24]. When the metallic cations gradually accumulate and approximate saturation in MEA, leading to a gradual increase of voltage at constant stack current and holds stably (see in Fig. 2). After recovery, the content of Cu and Ca almost approximates that of MEA-0, whereas Fe element shows lower relative intensity in Fig. 8(c), which indicates that the concentration of the elements content obviously decreases in the MEA-7800 Renewed after being recovered with dilute sulfuric acid. The residual cations have little influence on cell performance (see in Figs. 3,4).

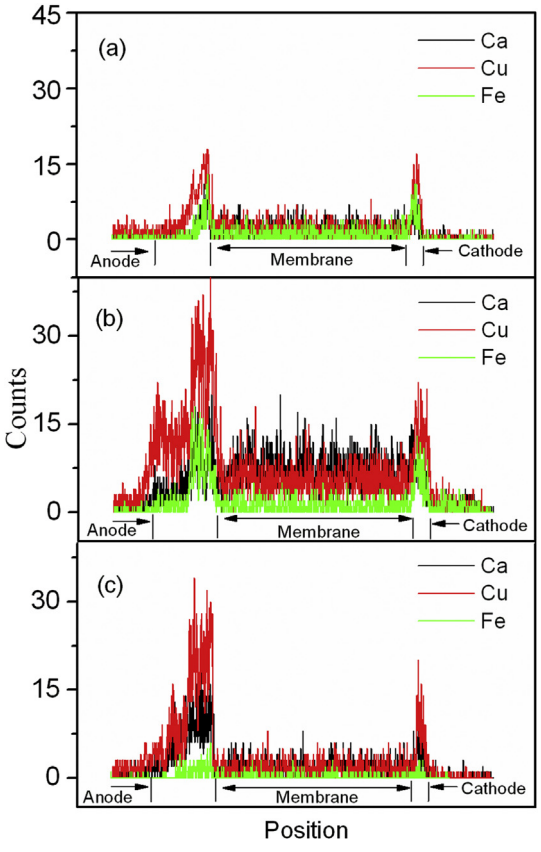

Fig. 8. Distribution of cations impurities in the cross-section of (a) MEA-0; (b) MEA-7800 and (c) MEA-7800 Renewed.

Table 2
The content of cations in the water of tank at 0 h and 7800 h.

Cation	0 h, Content/mg L^{-1}	7800 h, Content/mg L^{-1}
Ca	0.0441	0.0703
Cu	0.0054	0.057
Fe	0.0023	0.011

In addition, Cu and Fe still exist in other forms in the cathode catalyst layer. Cu^{2+} has quite positive Nernst potential and can be easily reduced to Cu at the cathode, which could cover with catalyst and block the active sites of platinum [31]. Moreover, Nernst potentials of Fe^{3+} is −0.01 V vs. SHE, so underpotential deposition (UPD) could happen at the cathode [32]. As a result, the cations impurities can occupy the cathode catalytic sites and hinder the delivery channel of protons of Nafion polymer electrolyte and membrane, which will not only increase ohmic resistance but also lead to the increase in charge transfer resistance, as given in Fig. 5.

3.8. Inductance coupling plasma spectroscopy (ICP) analysis

The factors that led to the increase in the cations content were revealed through analyzing the feed water of tank at 0 h and 7800 h by means of ICP. Table 2 listed the cationic content of the feed water. Table 2 shows that there was a considerable accumulation of the metallic cations in the feed water with the process of water electrolysis, and the cations of Cu, Ca and Fe were obviously increased.

The cations found should originate in part from the deionized water supplied for the experiment (see in Table 2). The cations were concentrated with the water being electrolyzed and added from time to time with refilling the tank. The cations may originate from other sources, such as water tank, the piping and other components of the electrolysis unit, which were made of stainless steel and copper. The trace mount of cations impurities could be dissolved by circulating water. As a result, ion-exchange processes take place in the stack between circulating water and electrolyzer, and the metallic cations enter into water electrolyzer and gradually accumulate in catalyst layer and membrane, resulting in the increased voltage. When the cations impurities get equilibrium in the catalyst layer and membrane, the electrolysis voltage arrives at a steady state, as shown in Fig. 2.

In order to maintain the stable performance of water electrolyzer, it is important that the electrolysis stack and system's pipelines should be made of corrosion-resistant material and high purified feed water should be used. Meanwhile, it is preferable that the water quality is measured online.

4. Conclusions

A nine cell PEM electrolyzer stack was developed and tested for 7800 h. Under a constant current mode, the stack voltage was found to increase at the rate of 0.589 mV h^{-1} before 4805 h, then decrease to a great extent and reach stable. The stack performance was degraded severely in the presence of Ca, Cu and Fe impurities. By the characterization techniques, the stack performance degradation was mainly attributed to the metallic cations poisoning, such as Ca, Cu and Fe. The cations occupied ion exchange sites in the Nafion polymer electrolyte of membrane and the catalyst layers, resulting in the increase in ionic resistance and charge transfer resistance, which would lead to the increase in the anode and cathode overpotential. The cations impurities should originate in part from the feed water, other sources were the water tank, the piping and other components of the electrolysis unit. In addition, the hydrogen crossover current density of the membrane slightly increased after 7800 h operation, which should result from the membrane thinning down. So the degradation of the PEM electrolyzer stack was reversible and could be almost recovered to the initial performance by using dilute sulfuric acid.

Acknowledgment

We thank the National High Technology Research and Development Program of China (863 Program, 2013AA110201) and the Natural Science Foundations of China (No. 21306190) for financial support.

References

[1] F. Barbir, Sol. Energy 78 (2005) 661–669.
[2] C.S. Song, Top. Catal. 49 (2008) 1–3.
[3] A.H.K. Abdel, M.A. Shalabi, Int. J. Hydrogen Energy 17 (1992) 359–367.
[4] http://dx.doi.org/10.1016/S1464-2859(04)00213-5.
[5] http://www.plantservices.com/vendors/products/2009/080.html.
[6] G.B. Chen, H.M. Zhang, H.X. Zhong, H.P. Ma, Electrochim. Acta 55 (2010) 8801–8807.
[7] S.D. Song, H.M. Zhang, X.P. Ma, Z.G. Shao, Y. Zhang, B.L. Yi, Electr. Commun. 8 (2006) 399–405.
[8] S.A. Grigoriev, P. Millet, S.A. Volobuev, V.N. Fateev, Int. J. Hydrogen Energy 34 (2009) 4968–4973.
[9] B. Marco, G. Daniel, J. Electrochem. Soc. 144 (1997) 573–581.
[10] E. Rasten, G. Hagen, R. Tunold, Electrochim. Acta 48 (2003) 3945–3952.
[11] A. Marshall, B. Borresen, G. Hagen, Mater. Chem. Phys. 94 (2005) 226–232.
[12] H.C. Ma, C.P. Liu, J.H. Liao, Y. Su, X.Z. Xue, W. Xing, J. Mol. Catal. A. Chem. 247 (2006) 7–13.
[13] P. Millet, T. Alleau, R. Durand, J. Appl. Electrochem. 23 (1993) 322–331.
[14] P. Millet, R. Ngameni, S.A. Grigoriev, N. Mbemba, F. Brisset, A. Ranjbari, C. Etiévant, Int. J. Hydrogen Energy 35 (2010) 5043–5052.
[15] Ö.F. Selamet, F. Becerikli, M.D. Mat, Y. Kaplan, Int. J. Hydrogen Energy 36 (2011) 11480–11487.
[16] G.Q. Wei, Y.X. Wang, C.D. Huang, Q.J. Gao, Z.T. Wang, L. Xu, Int. J. Hydrogen Energy 35 (2010) 3951–3957.
[17] F.J.R. Varela, O. Savadogo, J. New. Mater. Electrochem. Syst. 9 (2006) 127–137.
[18] X. Yuan, H. Wang, J. Colin Sun, J. Zhang, Int. J. Hydrogen Energy 32 (2007) 4365.
[19] J. Cheng, H. Zhang, G. Chen, Y. Zhang, Electrochim. Acta 54 (2009) 6250.
[20] I.D. Raistrick, Electrochim. Acta 25 (1990) 1579.
[21] M. Eikerling, A.A. Kornyshev, J. Electroanal. Chem. 475 (1999) 107.
[22] L.S. Zhang, X. Jie, Z.G. Shao, X.Y. Wang, B.L. Yi, J. Power Sources 241 (2013) 341–348.
[23] X. Jie, Z.-G. Shao, J. Hou, G. Sun, B. Yi, Electrochim. Acta 55 (2010) 4783.
[24] B.L. Kienitz, H. Baskaran, T.A. Zawodzinski Jr., Electrochim. Acta 54 (2009) 1671.
[25] E. Slavcheva, R. Vitushinsky, W. Mokwa, U. Schnakenberg, J. Electrochem. Soc. 151 (2004) E226–E237.
[26] L.A. Da Silva, V.A. Alves, A.P. Da Silva, S. Trasatti, J.F.C. Boodts, Acta 42 (1997) 271–281.
[27] S.S. Kocha, J.D. Yang, J.S. Yi, AICHE. J. 52 (2006) 1916–1925.
[28] T. Okada, J. Electroanal. Chem. 465 (1999) 1.
[29] X. Cheng, Z. Shi, N. Glass, L. Zhang, J. Zhang, D. Song, Z.-S. Liu, H. Wang, J. Shen, J. Power Sources 165 (2007) 739.
[30] X. Jie, Z.-G. Shao, B. Yi, Electrochem. Commun. 12 (2010) 700.
[31] X. Jie, J. Hou, Z.-G. Shao, B. Yi, Electrochemistry 15 (2009) 212–214.
[32] E.R. Kotz, S. Stucki, J. Appl. Electrochem. 17 (1987) 1190–1197.